particles

MDPI

Article

ICARUS at the Short-Baseline Neutrino Program: First Results †

Maria Artero Pons on behalf of the ICARUS Collaboration

INFN Sezione di Padova, University of Padova, Via Marzolo 8, 35131 Padova, Italy; maria.arteropons@pd.infn.it

† This paper is based on the talk at the 13th International Conference on New Frontiers in Physics (ICNFP 2024), Crete, Greece, 26 August–4 September 2024.

Abstract: The ICARUS collaboration employed the 760-ton T600 detector in a successful three-year physics run at the underground LNGS laboratory. In 2021, ICARUS started its new operation at Fermilab, collecting a substantial amount of neutrino events from the Booster Neutrino Beam (BNB) and the neutrinos at the Main Injector (NuMI) beam off-axis. These were used to test the ICARUS event selection, reconstruction, and analysis algorithms. ICARUS successfully completed its commissioning phase in June 2022, moving then to data taking for neutrino oscillation physics, aiming at first to either confirm or refute the claim by the Neutrino-4 short-baseline reactor experiment. ICARUS will also perform measurements of neutrino cross sections in LAr with the NuMI beam and several Beyond Standard Model studies. After the first year of operations, ICARUS will search for evidence of sterile neutrinos jointly with the Short-Baseline Near Detector, within the Short-Baseline Neutrino program. In this work, preliminary results from the ICARUS data with the BNB and NuMI beams are presented, both in terms of the performance of all ICARUS subsystems and the capability to select and reconstruct neutrino events.

Keywords: neutrino physics; liquid argon; detector performance; event selection; cross section; long-lived particles

Academic Editors: Larissa Bravina, Sonia Kabana and Armen Sedrakian

Received: 30 December 2024
Revised: 31 January 2025
Accepted: 9 February 2025
Published: 14 February 2025

Citation: Artero Pons, M., on behalf of the ICARUS Collaboration. ICARUS at the Short-Baseline Neutrino Program: First Results. *Particles* **2025**, *8*, 18. https://doi.org/10.3390/particles8010018

1. Introduction

Anomalies from accelerator experiments (LSND and MiniBooNE), reactors, and radioactive sources have been reported in the last 20 years, unable to fit inside the three-flavor oscillation scheme [1]. These results suggest the existence of a new sterile neutrino state, characterized by an eV-scale mass state and by a small mixing to the active flavors, that would drive short-distance oscillations. Recent results from the reactor Neutrino-4 collaboration [2] have also shown a hint of an oscillatory signature, which could be associated with sterile neutrinos. The existing anomalies are currently under investigation by dedicated neutrino oscillation experiments, providing exciting yet partially contradictory results on the active–sterile scenario. Thus, a coherent general description is far from being complete.

The Short Baseline Neutrino (SBN) program [3] based at Fermilab is designed to address the possible existence of eV mass-scale sterile neutrinos in both appearance and disappearance channels. It consists of large Liquid Argon Time Projection Chambers (LArTPCs) sitting along the Booster Neutrino Beam (BNB), where near and far detector locations have been optimized to achieve world-leading sensitivity in the search for $\nu_\mu \rightarrow \nu_e$ signals. The joint effort will enable the coverage of the full LSND 99% C.L. allowed region at $\sim 5\sigma$ studying the ν_e appearance, while at the same time performing a sensitive search in the ν_μ disappearance channel.

Neutrino energy spectra seen from both detectors are almost identical; however, due to the narrower solid angle seen by the far detector with respect to the near one and its different

active mass, the number of neutrino interactions expected at the near detector for the same proton-on-target exposure is nine times higher than at the far detector (neutrino flux expectations for different detector locations can be found in Figure 3 of Ref. [3]). Neutrino spectra are virtually identical for the near and far detectors, as are the interaction cross sections; consequently, the associated systematic uncertainties are expected to cancel out in the near–far comparison. Furthermore, given the same detection technology, many detector systematic uncertainties nearly cancel out as well when comparing the measurements at both locations. On top of that, the superb detector capabilities of the LArTPC technology allow a unique identification and reconstruction of neutrino interactions together with an efficient rejection of background events, particularly from neutral current interactions.

ICARUS is the far detector of the program, located at 600 m from the Booster target. In addition to the BNB neutrinos, ICARUS is also exposed $\sim 6^\circ$ off-axis to the higher energy neutrinos from the Main Injector (NuMI) beam, where most of the events are in the 0–3 GeV energy range and have an enriched component of ν_e (few %). The analysis of these events will provide an independent cross-check to the BNB oscillation results when testing the Neutrino-4 results. In parallel, Beyond the Standard Model searches and neutrino–argon cross-section measurements will be conducted, playing a crucial role in oscillation analysis and systematic constraints, particularly focusing on energies relevant to the future long-baseline experiment, such as the multikiloton DUNE LArTPC detector.

The near detector has just started physics operation, receiving its first neutrinos in July 2024 and has resumed physics data taking in December 2024 after the summer shutdown. However, the ICARUS-standalone phase is addressed to test the recent Neutrino-4 oscillation claim, exploiting its $\sim$ mm 3D reconstruction and excellent calorimetric capabilities. The Neutrino-4 oscillation-like signal for $\bar{\nu}_e$ events can be initially investigated in ICARUS with the BNB searching for a ν_μ disappearance as a function of the neutrino energy. Analogous, more direct searches for ν_e disappearance using the NuMI beam will follow.

In this work an up-to-date review of the current status of ICARUS and its first results will be given.

2. The SBN Far Detector: ICARUS

The ICARUS-T600 cryogenic detector is the first large-scale operating LAr-TPC containing 760 tons of ultra-pure LAr, of which 476 tons are active (the active liquid argon volume is commonly referred to as the instrumented region of the detector where the signal is read out [3]). It consists of two large and identical adjacent modules with internal dimensions of 3.6 (W) $\times$ 3.9 (H) $\times$ 19.6 (L) m^3. Each module houses two LAr-TPCs separated by a common central cathode with a maximum drift distance of 1.5 m, equivalent to 0.96 ms drift time at the nominal 500 V/cm electric drift field. The anode of each TPC is composed of three parallel wire planes placed 3 mm apart from each other and oriented at 0° and $\pm 60^\circ$ with respect to the horizontal direction. The ICARUS light detection system is equipped with 360 8-inch diameter photomultiplier tubes (PMT) placed behind the anode planes. They are used to detect the prompt LAr scintillation light for the purpose of event triggering and absolute timestamping of the recorded events, reconstructing the interaction position along the drift coordinate.

In 2013, ICARUS concluded a very successful 3-year-long data-taking at the underground Gran Sasso National Laboratories (LNGS), being exposed to the CERN to Gran Sasso (CNGS) neutrino beam, demonstrating the full maturity of the LArTPC technique. In contrast to the clean and noiseless environment in which ICARUS operated underground [4], the SBN program offers a completely different venue. The shallow depth at which ICARUS functions at FNAL exposes the detector to an abundant flux of cosmic rays, which would overwhelm the detector, as these can induce several additional and

uncorrelated triggers during the 1 ms drift time. On average, ∼11 cosmic tracks are expected to cross the entire detector volume during each drift window, which need to be identified and suppressed. To cope with this challenging condition, the detector setup includes a ∼3 m concrete overburden to reduce the cosmic ray flux, complemented by a ∼4π coverage cosmic ray tagger (CRT) system to tag the remaining incoming charged particles. The overburden is expected to reduce the dominant muon flux by ∼25%, filtering out muons with kinetic energy below 1.5 GeV. There is a more effective suppression for primary hadrons, with a reducing factor of ∼500 for protons and ∼200 for neutrons, while the electromagnetic cosmic ray component is almost fully eliminated. More details about the expected flux reduction due to this passive shielding can be found in Ref. [5]. In addition, the coincidence of the CRT signal with the light and charge signals of the chamber is also exploited to further suppress the backgrounds. Cosmic background rejection strategies are of utmost relevance for the $\nu_\mu \longrightarrow \nu_e$ channel, as the oscillation study relies on the tiny intrinsic ν_e component in the BNB beam. Any additional contribution of background faking ν_eCC interactions would negatively affect the oscillation sensitivity.

3. ICARUS Data Taking at Fermilab

After the arrival of ICARUS at FNAL in August 2018, all subsystems were installed in the detector, and the correct operation of its components was verified. Cryogenic commissioning started in January 2020, and detector activation took place on 27 August 2020 when the TPC wire planes and the cathode high voltage were taken to nominal voltage. The CRT system consists of a top, side, and bottom scintillator panel subsystems, which were installed through the commissioning activities, but culminated in December 2021 with the placement of the last top CRT panel. ICARUS was first fully operational in June 2021, when the first neutrinos were collected, and took data stably with BNB and NuMI beams in parallel with commissioning activities. The overburden installation started once the Top CRT commissioning was completed and was finalized on 7 June 2022, marking the beginning of the ICARUS physics data-taking phase. Top CRT cosmic rates were monitored during the commissioning phase, showing a factor of ∼2 reduction due to the overburden installation. Further details about its first operation activities can be found in Refs. [6,7]. During ICARUS physics runs, data are collected from both BNB and NuMI beams, triggering events whose scintillation light is detected in coincidence with the proton beam extraction signal. The collected beam statistics for all physics runs are summarized in Table 1, showing the duration of each run, the total amount of protons on target (POT) collected, and the beam run configuration. Note that during the Run-3 period, the NuMI beam ran in reverse horn current configuration (negative focusing), enhancing the antineutrino beam component.

Table 1. Collected beam statistics for Runs 1, 2, and 3 periods. Values are shown in proton on target (POT) units. For reference, around 1.2×10^5 ν are expected to be collected in ICARUS during 10^{20} POT.

Collected Protons on Target	BNB + Focusing	NuMI + Focusing	NuMI − Focusing
Run-1 (9 Jun–10 Jul 2022)	0.41×10^{20}	0.68×10^{20}	–
Run-2 (20 Dec 2022–14 Jul 2023)	2.05×10^{20}	2.74×10^{20}	–
Run-3 (15 Mar–12 Jul 2024)	1.36×10^{20}	–	2.82×10^{20}
Total	3.82×10^{20}	3.42×10^{20}	2.82×10^{20}

Throughout the whole data collection, ICARUS proved its ability to acquire data steadily: overall beam data collection efficiency exceeded 97% in the last physics run, with excellent performance on long runs at high repetition rates. No beam periods, in particular during the summer pause, provided an opportunity to carry out maintenance and improve-

ment activities to keep upgrading the detector, including LAr filter regeneration but also PMT and TPC hardware advancement.

The free electron lifetime (τ_{ele}) is crucial to monitor the liquid argon purity in the TPCs and to ensure a precise measurement of the energy deposition from the ionization charge signal of collected events. If τ_{ele} is below 3 ms, impurities prevent an efficient detection and reconstruction of ionizing events inside the active volume. On the other hand, the higher the τ_{ele}, the better, as the probability that an ionization electron is captured by any impurity decreases. The LAr purity is continuously monitored by measuring the charge attenuation along the drift path of the electron ionization signals generated by cosmic ray tracks crossing the detector, which are used as standard candles. The evolution of τ_{ele} values can be seen in Figure 1 through the whole life of the ICARUS detector, showing a stable and adequate value for physics runs thanks to the cryogenic and purification systems. During Run-3, values were around 7–8 ms, allowing an almost full track detection efficiency in the whole 1.5 m drift (∼1 ms), which is equivalent to ∼40 parts per trillion of O_2 residual impurities in LAr.

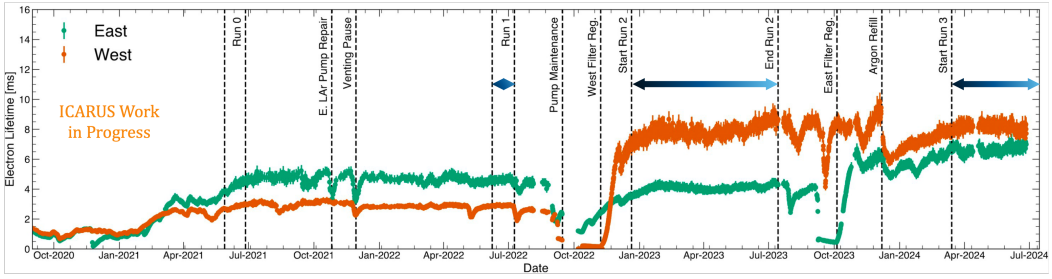

Figure 1. Electron lifetime evolution during ICARUS operations, where values for both cryostats are shown, together with indications of relevant events (e.g., filter Reg. refers to the regeneration of a liquid argon filter in the indicated module). Horizontal arrows highlight physics run periods.

4. Detector Calibration and Performance

ICARUS is exploiting all the available event statistics to characterize detector effects and improve its performance towards first physics results. In particular, two main works have been performed, exploiting the copious number of cosmic ray muons collected during Runs 1 and 2.

4.1. Calibration and Simulation of Ionization Signal and Electronics Noise

The goal of this study was to equalize charge measurements in data and tune the simulated TPC noise and signal shapes accordingly to reduce data-simulation discrepancies. The first item is relevant to ensuring a uniform TPC response to charge in space and time, which is usually expressed in terms of charge per length (dQ/dx) of hits along particle tracks and showers. Each TPC wire is instrumented to collect and digitize ionization charge while maximizing the signal-to-noise ratio). Signals are run through a signal processing chain that subtracts noise that is coherent across wires in the same readout board and deconvolves the signal to provide a Gaussian shape for ionization charge. These signals provide the input to reconstruction algorithms, which group together hits into tracks and electromagnetic showers for use in analysis. The reconstruction applied here is supplied by the Pandora framework [8].

The dQ/dx obtained might substantially differ from the original dQ/dx at the location where the ionization occurred; hence, it needs to be corrected before charge deposition is converted into energy loss for further studies. A number of effects perturb the charge response in ICARUS (argon impurities, drift field distortions, diffusion, wire plane intransparency, and channel gain variation), so a three-step equalization strategy was developed: a first equalization in the drift direction, a second equalization in the two wire plane di-

rections, and a third and final TPC equalization. The characterization of noise in data is also important for understanding its impact on ionization signals and the reconstruction of particle interactions in the detector volume. ICARUS TPC noise has been characterized principally through measurements of the absolute noise scale, frequency characteristics, and channel-to-channel correlations. These signal shape and noise model measurements are used as input to a data-driven model to obtain an accurate and complete Monte Carlo simulation (MC).

Figure 2 shows the comparison of the signal shape measurement in the collection plane from data and Monte Carlo simulation generated with and without the tuning applied to validate the presented results. More details can be found in Ref. [9].

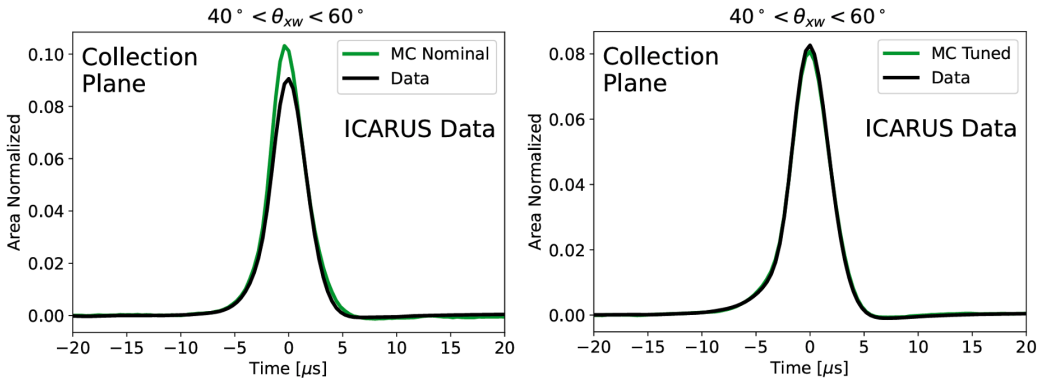

Figure 2. Comparison of the signal shape measurement between data and MC simulation for a particular track inclination θ_{xw}. θ_{xw} is the angle of the track projected in the $\hat{x}$-$\hat{w}$ plane with respect to the $\hat{w}$, where $\hat{x}$ is the drift direction of the ionization electrons in the TPC and $\hat{w}$ is the direction perpendicular to the wire orientation within the wire plane. See Figure 2 of Ref. [9] for a graphic explanation. The left plot shows the nominal (untuned) simulation, while on the right the comparison is conducted after the tune [9].

4.2. Angular Dependent Measurement of Electron–Ion Recombination for Ionization Calorimetry

Precise tracking and calorimetric information are extracted from the collected electrons ionized from argon by charged particles crossing the detector. These electrons are drifted from their point of production by a large electric drift field to a set of readout wire planes that measure the charge. However, depending on the charge density of the medium, a significant fraction of ionization electrons recombine with stationary clouds of argon ions, decreasing the amount of charge measured. The rate of recombination has a non-linear dependence on the energy per length (dE/dx) deposited by charged particles. In addition, because the drift electric field points in a specific direction, the recombination process may depend on the angle of the ionizing track to the electric drift field. Measuring the rate of recombination across relevant variables is necessary for LArTPC detectors to precisely leverage calorimetry for particle identification and energy reconstruction and is also of particular interest for argon-based dark matter detectors. This work has thus been applied in the absolute energy scale, calibration taking advantage of the previous calibration and simulation advances. The electron–ion recombination measurement is performed by fitting the electronics gain and recombination parameters in a single and self-consistent fit. This included minimum- and highly-ionizing depositions from cosmic ray muons and protons from NuMI neutrino interactions to anchor the gain and supply the necessary information to account for the non-linearity of recombination, respectively.

The recombination-modified box model [10] is taken as a starting point, being described as $\frac{dQ}{dx} = \log\left(\alpha + \mathcal{B}\frac{dE}{dx}\right)/\mathcal{B}W_{\text{ion}}$ with $\mathcal{B} = \beta/\mathcal{E}\rho$. Here, $\mathcal{E}$ is the electric field, ρ the Ar density, W_{ion} the argon ionization work function, and α and β are parameters of

the fit. The angular dependence is studied through the β parameter, examining three different models: constant ($\beta(\phi) = \beta(90°)$), columnar ($\beta(\phi) = \beta(90°)/\sin\phi$), and ellipsoid ($\beta(\phi) = \beta(90°)/\sqrt{\sin^2\phi + \cos^2\phi/R^2}$, with R another fit parameter), where ϕ is the angle of the track to the drift electric field.

The results showed a significant angular dependence in recombination for highly-ionizing particles in LAr, confirming a preference for the ellipsoid modified box model. This model was the only one capable of describing the data across all measured track angles with respect to the drift electric field. Figure 3 left compares these three models, showing the measured ratio of $\beta(\phi)$ normalized to a specific angular range. The ellipsoid model fit is able to describe the angular dependence across different track inclinations, while neither the constant nor the columnar models match the dependence.

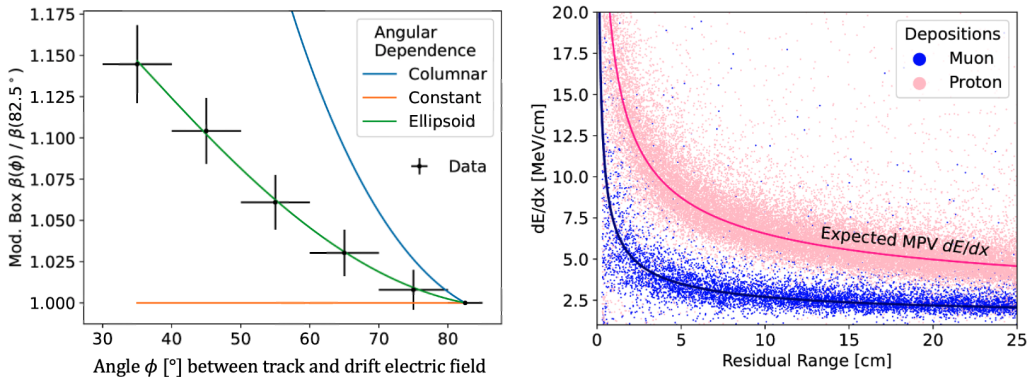

Figure 3. Left: Ratio of $\beta(\phi)$ measurements in the modified box fit to a reference value for three models of track angular dependence. **Right**: Calibrated energy depositions from selected stopping muons and protons in ICARUS data as a function of residual range, i.e., distance to the end point of a track (from Ref. [11]).

This calibration (electron–ion recombination and electronic gain measurements) enables the use of calorimetric particle identification and energy reconstruction. The rightmost in Figure 3 shows the distribution of calibrated energy depositions for selected stopping muons and protons, proving both the accuracy of the calibration (data match theoretical expectations) and the ability to calorimetrically separate muon and proton tracks leveraging their characteristic Bragg peak. A complete discussion of the obtained results can be found in Ref. [11].

4.3. Validation Studies

Several validation studies have been performed to further scrutinize the detector performance and energy scale calibration. The first one focuses on the comparison between two different methods of stopping proton kinetic energy reconstruction: one by calorimetry (summing up charge associated with energy deposition along the track), E_{calo}, and another by range (converting the total reconstructed length of the stopping proton track to kinetic energy via a look-up table), E_{range}. The result of this cross-check is presented in Figure 4 (left), showing some bias between the two methods and a resolution of about ∼5% for protons in data. Further studies using data from muon tracks and comparisons with simulations demonstrated good modeling of minimum ionizing depositions but indicated larger fluctuations in electron–ion recombination for highly ionizing energy depositions than those currently simulated.

ICARUS capabilities in electromagnetic shower reconstruction can be tested using a sample of events with π^0 mesons produced in neutrino interactions. The decay of a particle with known mass gives a good handle to test detector energy calibration. To simplify the scenario, $1\mu1\pi^0$ events (a subset of the ν_μ CC channel) coming from the BNB were selected.

The reconstructed neutral pion invariant mass showed a small electromagnetic shower energy scale bias (∼3%) and a ∼10% shower energy resolution [12].

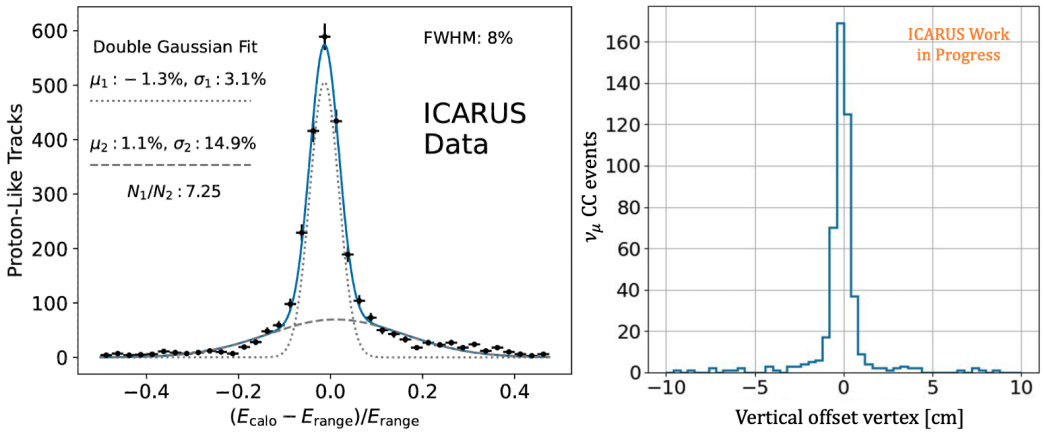

Figure 4. Left: Comparison of calorimetric and range energy reconstruction for selected protons in ICARUS data (from Ref. [11]). **Right**: Distribution of the difference between the scanned and automatically reconstructed neutrino vertex y positions for a sample of hand-scanned events.

Finally, a dedicated visual study of events was performed, selecting a sample of ν_μ CC interactions from BNB in the active LAr to allow a first validation of the Pandora reconstruction algorithm. These events were further exploited to develop an automatic event selection procedure and to evaluate its performance in terms of efficiency and purity. For each visually scanned event, the 3D position of the vertex and end muon position were saved and compared with the automatic reconstruction variables, which helped identify major issues in event reconstruction. As an example, in ∼90% of these events, the reconstruction reasonably identified the neutrino interaction vertex position, meaning the difference in each direction between the two estimates was within 3 cm; see, as an example, Figure 4 (right).

4.4. Detector Performance

After the detector calibration and its validation, it is possible to assess the detector performance by carrying out different tests.

One possibility is to leverage the correlation between CRT and PMT signals to effectively identify incoming cosmics or exiting particles. PMT calibrations are performed on a regular basis to ensure a precise and stable timing equalization (∼300 ps) [13]. The CRT system was precisely calibrated in order to allow accurate relative synchronization (∼ ns) between CRT and PMT subsystems through a global trigger signal distributed among the different sub-detectors. This synchronization enables the possibility to associate each reconstructed optical flash with one or more CRT hits, using only time information. The association is performed looking for CRT hits within 100 ns of a PMT flash and computing a simple time difference, $T_{\mathrm{CRT}} - T_{\mathrm{PMT}}$, obtaining a powerful tool to perform a preliminary classification of the interaction prior to the TPC reconstruction.

As schematically shown in Figure 5 (left), if the $T_{\mathrm{CRT}} - T_{\mathrm{PMT}}$ is negative, the CRT hit was seen before the PMT activity; hence, the associated particle entered the detector from the outside. On the other hand, a positive value will indicate that the light was detected before the CRT hit, and thus the particle first produced light inside the detector and then exited. In addition, the CRT-PMT classification is also able to exploit the relative timing with respect to the beam gate opening, precisely determining if the flash under study happened during the spill time or not. For instance, by selecting events with optical flashes in time with the beam spill and not matched with any CRT hit, an enhanced sample of fully contained neutrino interactions is expected, effectively suppressing the cosmic-

induced background in time with the beam. Comparing the off-beam and on-beam data distributions of $T_{CRT} - T_{PMT}$ for the top CRT, a significant excess is observed at positive values for on-beam data (Figure 5 (right)), demonstrating that CRT-PMT matching can help disentangle cosmic tracks from beam-induced activity. This technique can additionally distinguish different topologies of tracks entering and exiting the detector. For example, a single flash can be matched to both a top and side CRT hits, before and after the PMT flash respectively identifying through-going tracks that can be used to cross check the TPC reconstruction.

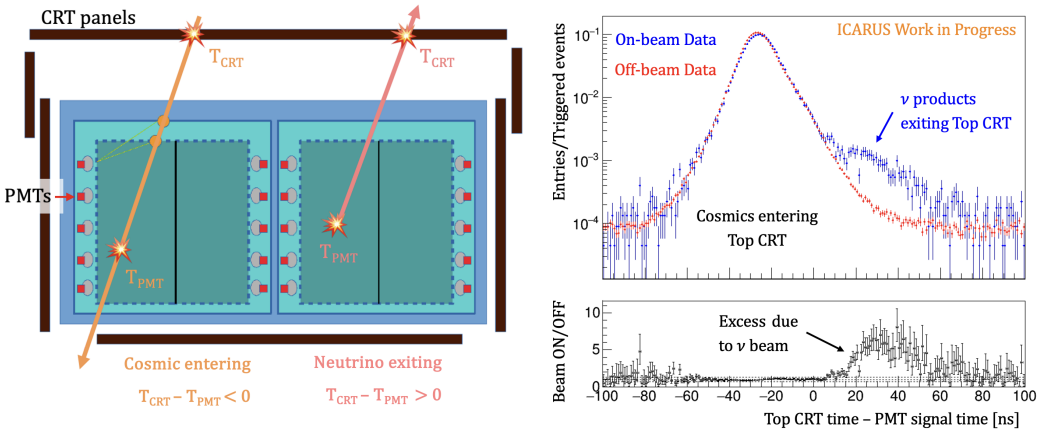

Figure 5. Left: Schematic drawing showing a way to distinguish between tracks entering and exiting the ICARUS cryostat, using the CRT-PMT timing correlation. **Right**: CRT-PMT signal time for Top CRT using on-beam and off-beam data to highlight beam-related activity exiting the detector.

Another option to test the detector performance is to reconstruct the neutrino beam bunch structure and exploit its characteristic time profile. BNB and NuMI have different neutrino energy spectra but share a similar beam structure. Each proton pulse has a ≈53 MHz substructure with 81 buckets every ∼19 ns. Other than the difference in energy range between BNB and NuMI beam, NuMI has six batches per spill, while BNB has only one. A batch is a sequence of 81 buckets, at a rate of ≈53 MHz, hence BNB has a 1.6 µs spill, 81 bunches, and 18.9 ns spacing (52.8 MHz), while NuMI has a 9.6 µs spill, 486 bunches (81 × 6), and 18.8 ns spacing (53.1 MHz). The time for protons to hit the target, the propagation and decay of mesons, and the travel time of neutrinos to the detector can be assumed to be a constant offset for all interactions. Hence, the neutrino at the upstream detector wall inherits the time profile of the proton bunches. This feature has two major applications: a selection time window around the beam bunches can reduce the fraction of cosmic background events, as these are uniformly distributed during the entire beam spill, while neutrinos are much more peaked. The strength of this cut depends on the allowed time window width around the neutrino peak, which also establishes the background rejection and neutrino selection efficiency. The second application expands the LArTPC capability to search for long-lived massive particles that have longer time of flight and reach the detector delayed with respect to neutrinos, leveraging events between neutrino bunches [14].

Resistive wall current monitors measure a current induced by the beam protons that reproduces accurately the proton pulse's longitudinal time profile. This provides a jitter-free reference signal that marks the time the first proton bunch hits the target (RWM time).

A first measurement was performed using light information only and will be repeated in the future, including charge data, which are expected to further improve the measurement resolution. The large number of PMTs on both sides of the modules allows for the reconstruction of the time of any scintillation event (t_ν) and provides its location across the length of the ICARUS detector. By applying a further correction to account for the time-of-flight (ToF, using the flashlight barycenter) and a CRT filter to remove any cos-

mic ray activity, it is possible to obtain the neutrino time profile at the same reference plane. Figure 6 shows the BNB bunch structure reconstructed with ICARUS data, where all 81 bunches were recognized. The NuMI beam profile was also studied, showing the 6 characteristic batches with its 81 inner peaks identified as well.

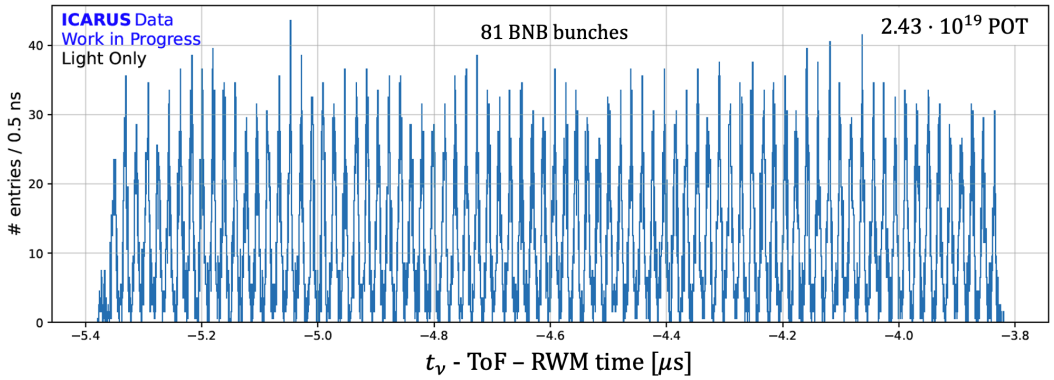

Figure 6. Neutrino arrival time (t_ν) distribution with respect to the proton beam extraction time (RWM time) after rejecting incoming cosmic rays and correcting for neutrino time of flight (ToF), showing the BNB beam bunch structure [15].

Each batch was fitted with a multigaussian fit to characterize the beam bunch structure separately for BNB and NuMI. The peak time position of each bunch correlated with its location inside the batch was used to measure the separation between two consecutive bunches. The results obtained were 18.935 ± 0.001 ns for BNB and 18.828 ± 0.003 ns for NuMI beams. Finally, using these measurements and by superimposing all the bunches, it was possible to evaluate the shape of the average bunch and determine its width, reporting 2.99 ± 0.04 ns and 3.11 ± 0.06 ns for BNB and NuMI, respectively, as shown in Figure 7; see more details in Ref. [15].

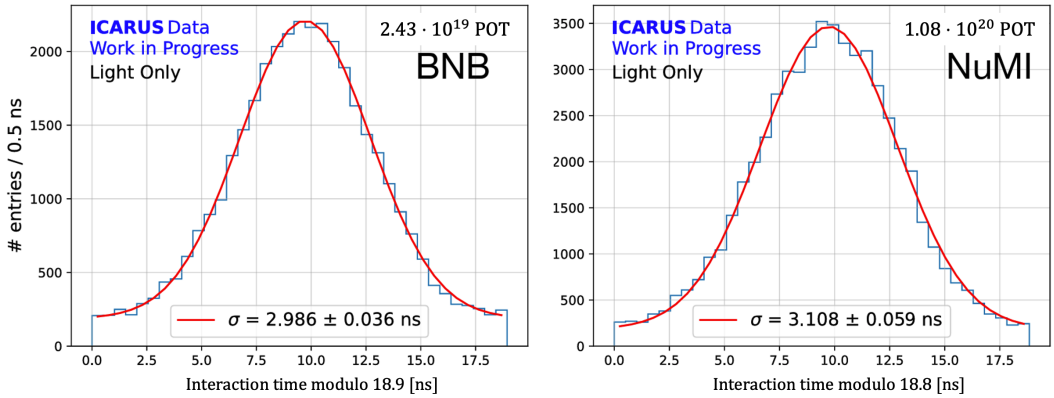

Figure 7. Event timing distribution of the 81 beam bunches merged with overlapped fit for BNB (**left**) and NuMI (**right**) beams [15].

5. ICARUS Stand-Alone Physics Program

5.1. 1μNp Event Selection Analysis with BNB

ICARUS has been taking data alone while waiting for the near detector to become fully operational. Even though the latter one has recently entered physics operation, ICARUS is addressing as a first test the Neutrino-4 oscillation claim alone. The Neutrino-4 oscillation-like signal for $\bar{\nu}_e$ events can be initially investigated in ICARUS with the BNB searching for the ν_μ disappearance as a function of the neutrino energy.

As a first step, studies have been performed on fully contained events with a simple topology: a single muon and at least one proton in the final state (1μNp events) exiting

from the same interaction vertex. An example can be seen in Figure 8 for a 1μ3p data event candidate.

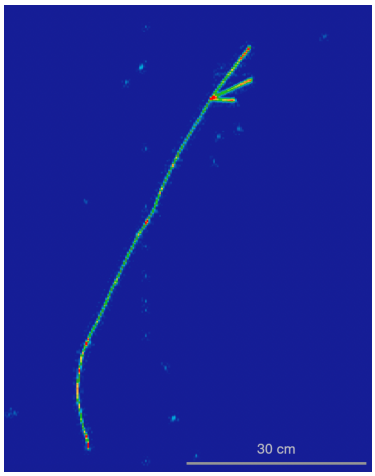

Figure 8. 1μNp candidate from BNB automatically selected, with three reconstructed proton candidates. The color scale all over the interaction is proportional to the ionization power of each particle, with red areas indicating where more deposited energy.

Due to the large amount of data to analyze, an automatic procedure to select signal events while rejecting cosmic rays is mandatory to handle the current statistics. Presently, the selection and reconstruction of neutrino candidates is performed using two independent analysis streams based on Pandora [8] pattern recognition and SPINE [16], a machine learning-based algorithm developed for ICARUS. Nonetheless, the selection procedure to recognize 1μNp events in both cases is based on similar criteria:

- TPC track associated with PMT light signal recorded inside the beam spill without any CRT signal in coincidence.
- Reconstructed vertex inside the fiducial volume: more than 25 cm apart from the lateral TPC walls and 30/50 cm from the upstream/downstream walls.
- All interaction-reconstructed objects are within 5 cm from the TPC active volume.
- Longest track ($\geq$50 cm) classified as muon by the particle identification tool (based on stopping power particle profiles).
- At least a proton with kinetic energy greater than 50 MeV (range-based measurement).
- No additional pions or photons.

The study of simulated events has allowed for the evaluation of the automatic selection efficiency and purity, reporting the following values: $\sim$80% purity for both reconstruction approaches and 50% and 75% efficiency for Pandora and SPINE, respectively. In addition to that, a small sample of data ($\sim 2 \times 10^{18}$ POT) was visually scanned to validate the performance of the reconstruction procedures, confirming the aforementioned results for both analyses.

To have a more complete analysis, all possible sources of systematic uncertainties were taken into account, including flux, cross-section, detector, and POT exposure errors. As a first approach, very conservative systematics have been adopted; for instance, detector uncertainties were evaluated by comparing calibrated with uncalibrated simulation samples. At present, flux/cross-section and detector systematics equally contribute to the total error band. Ongoing simulation improvements are expected to reduce residual data–MC discrepancies, decreasing the detector uncertainty contribution. Alongside, common systematic uncertainties are expected to cancel out when combining near and far detector data in future analyses.

Given that the signal is fully contained, the global kinematics of the events can be directly measured through the range of the involved particles. An example is shown in Figure 9 comparing the reconstructed neutrino energy for the selected 1μNp events in 10% of the Run-2 data with MC expectations, using both reconstruction approaches. A good agreement is observed within the total systematics in the two distributions. It is worth noting that the combination of all selection requirements results in a residual cosmic background contribution smaller than 1% from MC estimations.

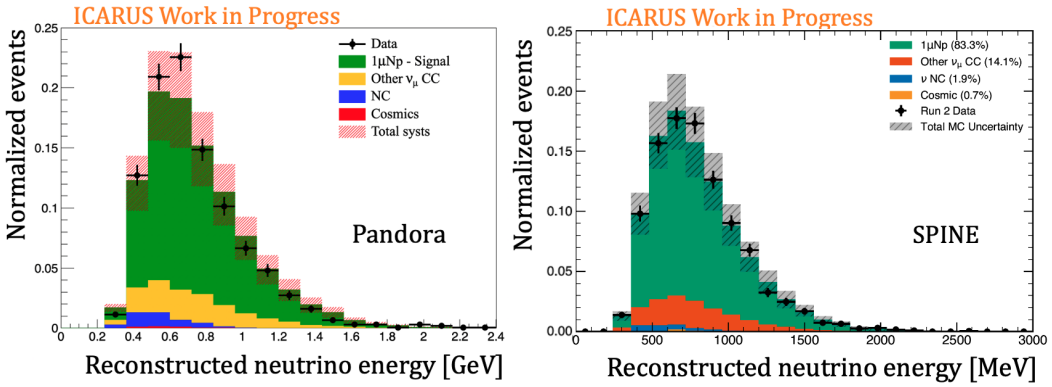

Figure 9. Plots showing a data/MC area normalized comparison of the reconstructed neutrino energy for 10% of data ($\sim$1.9 $\times$ 10^{19} POT). The Pandora reconstruction approach [17] is shown on the left, while the SPINE result [12] is on the right-hand side. Both reconstruction approaches have included a full treatment of systematic uncertainties.

The fact that only 10% of the data was analyzed is due to a blinding policy established within the ICARUS collaboration. This policy is designed to ensure that no bias is introduced during all physics analysis. The blinding process follows a structured set of steps, requiring permission to analyze increasing amounts of data. Ultimately, the process culminates in the opening of the signal box region, where the final analysis is performed. In this case, the presented 1μNp analysis was performed inside the first step. It is also common to define a control sample, being a suite of variables or interaction channels that are not strongly related to the sought signal, to be able to study a larger fraction of data and avoid any possible bias in the analysis.

At this stage and given the presented results, the next foreseen steps are to study the control sample, unblind the full dataset, and perform a single detector oscillation fit measurement.

5.2. Charged Current Mesonless Analysis with NuMI

Current long-baseline neutrino oscillation experiments report significant systematic uncertainties in their measurements. Some of the largest contributions come from the available models of nuclear physics processes, which distort neutrino–nucleus interactions with respect to their neutrino–nucleon interaction counterparts. These nuclear effects modify both the final-state particle kinematics and production content, altering the rate of detection of any given interaction channel as a function of all kinematic variables.

ICARUS is also sensitive to neutrinos produced by the NuMI beam, arriving from a 5.7° off-axis angle and coming from both pion and kaon decays, whose energy spectra span a few GeV. While NuMI statistics are expected to be much lower (around 332,000 ν_μ CC and 17,000 ν_e CC interactions are expected in ICARUS for a NuMI exposure of 6 $\times$ 10^{20} POT) than what SBND will provide in the BNB, the NuMI beam's energy spectrum provides a better-suited dataset for exploring interactions at neutrino energies closer to DUNE energy ranges. The energy range of NuMI ν_μ interactions in ICARUS is in a similar energy range to that expected by DUNE. The ν_e ICARUS spectrum instead covers DUNE's first oscillation

peak and provides good coverage of the relevant phase space. Moreover, a comparison of similar measurements in the NuMI and BNB beams can provide a direct probe of the energy dependence of neutrino interaction cross section.

Taking advantage of all these items, ICARUS is pursuing its first cross-section measurement targeting charged-current mesonless interactions with one muon and at least a proton as final state particles, but without producing any additional charged or neutral hadrons (CC0πNp). The signal definition of this analysis requires the interaction vertex to be in the fiducial volume, as previously defined, a single muon with more than 50 cm range, and a leading proton whose momentum is between 0.4 and 1 GeV/c, allowing any further number of protons given that the previous condition is met. Proton momentum range selection is based on several performed tests proving that short protons are very difficult to be reconstructed with good quality, while higher momentum protons are more likely to undergo strong interactions with nucleons and hence modify the particle identification power.

Typical variables of interest are the momenta of the muon and leading proton. No explicit requirement is applied to the containment of such tracks; thus, for exiting tracks, the momentum is estimated from multiple Coulomb scattering, while range-based measurement is used for all those that are contained. Other relevant quantities are related to different angles and transverse kinematic variables being a proxy for initial (i.e., Fermi motion) and final state information. In particular, since these variables are not reliant on contained tracks, they can still be well determined even when exiting tracks are present, and measurements are likely more robust to reconstruction failures.

Figure 10 shows two of these variables: the cosine of the angle between the muon and the leading proton ($\cos\theta_{\mu p}$) and the transverse momentum imbalance using only the leading proton (δp_T). Used statistics are 15% of ICARUS Run 1 and 2 NuMI beam data corresponding to the first step in the ICARUS blinding policy. In both plots, flux, interaction model, and detector systematic uncertainties have been carefully assessed. To ensure the robustness of the analysis, a study on the major background was performed, selecting events with undetected or misidentified charged pions. The so-called charged pion sideband is defined by requiring the presence of a second muon-like track of at least 10 cm. The study of this control sample with the same 15% of data showed good agreement within the systematics, as presented in Figure 11 left, demonstrating the readiness to study sidebands with full Run 1 and 2 event statistics. More information can be found in Ref. [18].

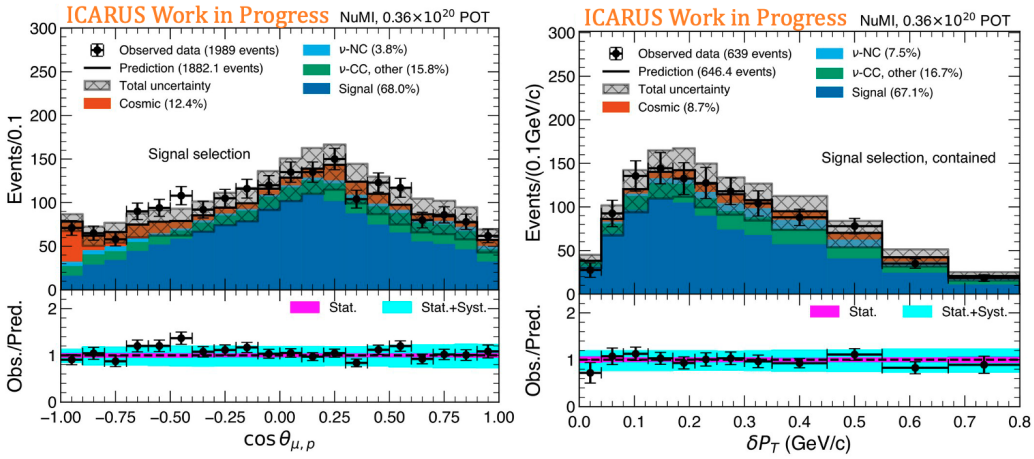

Figure 10. Cosine of the angle between the muon and leading proton candidate (**left**) and total transverse momenta (**right**) of selected signal events for 15% of data and MC samples [18].

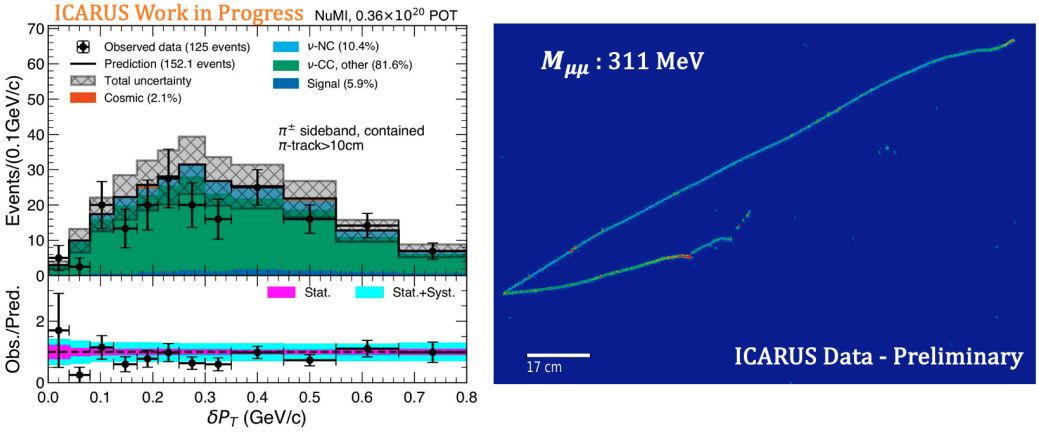

Figure 11. Left: Total transverse momenta distribution of pion-like sideband showing 15% of data compared with simulation (from Ref. [18]). **Right**: Example of di-muon data candidate identified with the selection described in the text, with red and cyan color scales indicating high and low energy depositions respectively.

5.3. Beyond Standard Model Search: Di-Muon Final State Topology

Several BSM physics models predict processes by which kaons ($K^{\pm}$ or K^0_L) decay to long-lived particles (LLP), which in turn decay to $\mu^+\mu^-$ pairs. Two such processes that have been considered so far are the Higgs portal scalar (HPS) [19], a dark sector model for dark matter, and a heavy QCD axion, or axion-like particles (ALP) [20], involving pseudo-scalar particles whose interactions happen by mixing with pseudo-scalar mesons. Under this scenario, kaons created in the NuMI beam would produce scalars that could then decay into di-muon pairs within the ICARUS detector. Calorimetric, topological, and kinematic features distinguish di-muon decays in the detector from neutrino backgrounds.

The presented analysis searched for di-muon decays in the fiducial volume where both muons were contained in the detector; see the example in Figure 11 (right). From detailed studies, background contributions come mainly from muon neutrino charged current coherent pion production. This ν_μCC-Cohπ is a rare neutrino scattering process where a ν_μ interacts with a nucleus (A) producing a muon and a pion in the forward direction. The coherent nature of the interaction (low transfer momentum) ensures that the nucleus remains intact and in its ground state. The process can be written as $\nu_\mu + \mathrm{A} \rightarrow \mu^- + \pi^+ + \mathrm{A}$. These interactions mimic the di-muon final state topology with $\mu^{\pm}\pi^{\mp}$, where the pion had been misidentified as a muon. An excess above the expected neutrino background in a narrow region of invariant mass consistent with a resonance peak would be a signature of new physics. Here the invariant mass is reconstructed from the observed muon pair, while the narrow region is defined to further reduce the background in the signal window.

The momenta of the predicted scalars is such that the di-muon products have a small opening angle; thus, a cut of 70° was imposed for this variable. In addition, kaons generally decay near the NuMI target; therefore, the momentum vector for most scalars points along the direction from the NuMI target to the ICARUS detector. The angle between these two vectors, the so-called θ_{NuMI}, is reconstructed as the angle between the summed di-muon momentum vector and the known direction from the NuMI target and the detector. The pointing resolution on this angle for scalar decays is ∼2°, while the distribution for neutrino interactions is much broader and peaked at ∼20°. These values were obtained with dedicated simulation studies based on the BSM model and were verified with data comparisons when possible, following the blinding policy. The full θ_{NuMI} was used in the analysis, distinguishing $\theta_{\mathrm{NuMI}} > 5°$ to characterize the background from $\theta_{\mathrm{NuMI}} < 5°$ to define the final signal selection region.

The search of signal events was performed as a "bump hunt" within the reconstructed di-muon invariant mass spectrum, which iteratively searched for any resonance and fit a scale factor to the dominant ν_μCC-Cohπ background component. The signal region search was performed in three steps: (1) di-muon mass window with the greatest excess above the nominal background is identified by the algorithm in the signal region $\theta_{\mathrm{NuMI}} < 5°$. (2) A scale factor in the ν_μCC-Cohπ background template is fit to data to increase background description accuracy in a larger $\theta_{\mathrm{NuMI}} < 10°$ region, but excluding the invariant mass range identified in the first step. (3) The algorithm is rerun again to identify the largest excess in the signal region, taking into account the scaled background.

The systematic uncertainties from the models used in the Monte Carlo simulation (flux, interaction cross sections, particle propagation, and detector response) influence the predicted event rates for signal and background channels. For that reason, a detailed and complete assessment of systematic uncertainties was performed and included in the analysis, with a rather conservative approach.

The final result of the search is shown in Figure 12 (left), analyzing data of 2.41×10^{20} POT collected with the NuMI beam between June 2022 and July 2023, corresponding to the full dataset of Runs 1 and 2. The initial background expectation in the signal box region was 7.8 ± 5.0 (syst.) $\pm$ 2.8 (stat.) events. Eight data events were observed, with the largest excess found in the mass window of $0.24 < M_{\mu\mu} < 0.31$ GeV, corresponding to a global significance of 0.19σ when compared with the null hypothesis. The excess was not statistically significant, and limits were set at the 90% confidence level. These results represent world-leading limits on heavy QCD axions for several choices of the muon and gauge boson couplings and leading limits among dedicated searches for the Higgs Portal scalar in the mass range $2m_\mu < M_S \lesssim 270$ MeV; see Figure 12 (right). This result is the first search for new physics performed with the ICARUS detector at Fermilab, paving the way for a future program of long-lived particles at ICARUS, as well as part of the Short-Baseline Neutrino program. See Ref. [21] for more details and further discussion.

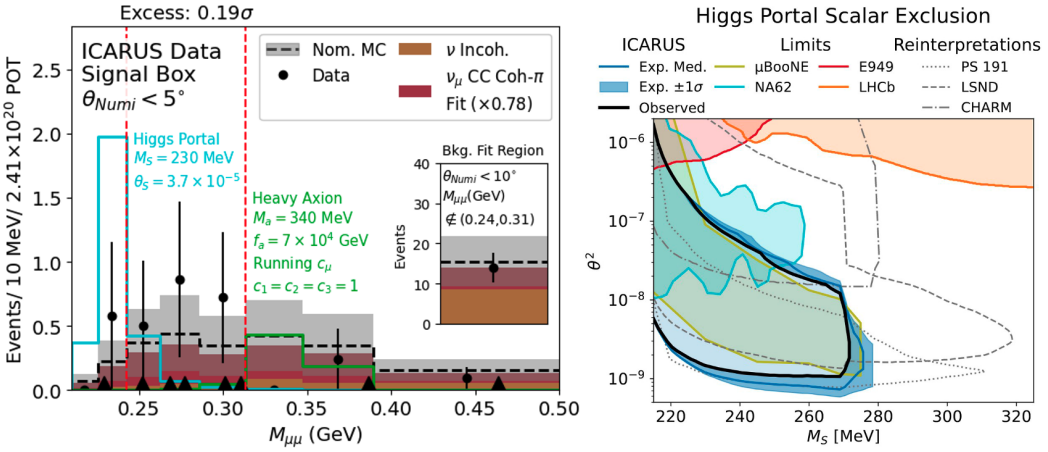

Figure 12. Left: Signal box result of the search showing the number of events identified as a function of the di-muon invariant mass. **Right**: Outcome on the Higgs Portal scalar model presenting the exclusion contour limits at the 90% CL, overlapped with other experiment results. The limits are shown on the scalar-Higgs mixing angle θ as a function of the Higgs Portal scalar mass. From Ref. [21].

6. Conclusions

ICARUS has been running smoothly in physics mode since June 2022, collecting neutrinos from both Booster and NuMI beams. Currently the detector is calibrated with cosmic muons and protons from neutrino interactions; the electronic response and physical properties of this have been carefully qualified and modeled in the simulation to resemble

the data. In addition, validation and performance studies have proved that ICARUS is able to precisely reconstruct interactions and exploit at its maximum all three detector subsystems to enhance neutrino identification and remove background contributions.

While waiting for the joint SBN operation, several single detector analyses have progressed, showing that ICARUS is well on the way for physics results. The test of the Neutrino-4 $\bar{\nu}_e$ oscillation hypothesis studying the ν_μ disappearance channel with BNB events is quite advanced, being ready to enlarge the control samples and perform a single detector oscillation fit. ν_μ-Ar cross-section measurements with the NuMI beam are in a similar stage, having demonstrated their capability to perform such calculations, and are now ready to analyze more data. Finally, the search for sub-GeV dark matter candidates in NuMI has been completed, presenting a first result for new particles decaying into two contained muons. No new physics signal was observed in either of the two studied models; thus, exclusion contour plots were set and shared with the scientific community.

Funding: This work was supported by the US Department of Energy, INFN, the EU Horizon 2020 Research and Innovation Program under the Marie Sklodowska-Curie Grant Agreement No. 734303, 822185, 858199, and 101003460, and the Horizon Europe Research and Innovation Program under the Marie Sklodowska-Curie Grant Agreement No. 101081478.

Data Availability Statement: The datasets presented in this article are not readily available. ICARUS Experiment at Fermilab Research Data Policies at https://icarus-exp.fnal.gov (accessed on 9 December 2024).

Acknowledgments: This document was prepared using the resources of the Fermi National Accelerator Laboratory (Fermilab), a U.S. Department of Energy, Office of Science, Office of High Energy Physics HEP User Facility. Fermilab is managed by Fermi Research Alliance, LLC (FRA), acting under Contract No. DE-AC02-07CH11359.

Conflicts of Interest: The author declares no conflict of interest.

Abbreviations

The following abbreviations are used in this manuscript:

BNB	Booster Neutrino Beam
CRT	Cosmic Ray Tagger
LArTPC	Liquid Argon Time Projection Chamber
NuMI	Neutrinos at the Main Injector
SBN	Short Baseline Neutrino

References

1. Acero, M.A.; Argüelles, C.A.; Hostert, M.; Kalra, D.; Karagiorgi, G.; Kelly, K.J.; Littlejohn, B.; Machado, P.; Pettus, W.; Toups, M.; et al. White paper on light sterile neutrino searches and related phenomenology. *J. Phys. G Nucl. Part. Phys.* **2024**, *51*, 120501. [CrossRef]
2. Serebrov, A.; Samoilov, R.; Chaikovskii, M.; Zherebtsov, O. The result of the Neutrino-4 experiment, sterile neutrinos and dark matter, the fourth neutrino and the Hubble constant. *arXiv* **2023**, arXiv:2302.09958.
3. Acciarri, R.; Adams, C.; An, R.; Andreopoulos, C.; Ankowski, A.M.; Antonello, M.; Asaadi, J.; Badgett, W.; Bagby, L.; Baibussinov, B.; et al. A proposal for a three detector short-baseline neutrino oscillation program in the Fermilab booster neutrino beam. *arXiv* **2015**, arXiv:1503.01520.
4. Rubbia, C.; Antonello, M.; Aprili, P.; Baibussinov, B.; Ceolin, M.B.; Barze, L.; Benetti, P.; Calligarich, E.; Canci, N.; Carbonara, F.; et al. Underground operation of the ICARUS T600 LAr-TPC: First Results. *J. Instrum.* **2011**, *6*, P07011. [CrossRef]
5. Behera, B.; ICARUS Collaboration. Cosmogenic background suppression at the ICARUS using a concrete overburden. *J. Phys. Conf. Ser.* **2021**, *2156*, 012181. [CrossRef]
6. Abratenko, P.; Aduszkiewicz, A.; Akbar, F.; Pons, M.A.; Asaadi, J.; Aslin, M.; Babicz, M.; Badgett, W.F.; Bagby, L.F.; Baibussinov, B.; et al. ICARUS at the Fermilab Short-Baseline Neutrino program: Initial operation. *Eur. Phys. J. C* **2023**, *83*, 467. [CrossRef] [PubMed]

7. Aduszkiewicz, A.; Bagby, L.; Behera, B.; Bernardini, P.; Bertolucci, S.; Betancourt, M.; Budd, H.; Boone, T.; Campos, A.; Casazza, D.; et al. Design and Implementation of the Cosmic Ray Tagger System for the ICARUS detector at FNAL. *arXiv* **2025**, arXiv:2501.03034.
8. Marshall, J.; Thomson, M. The Pandora software development kit for pattern recognition. *Eur. Phys. J. C* **2015**, *75*, 439. [CrossRef]
9. Abratenko, P.; Gurung, G.; Zennamo, J.; Richards, E.; Sapienza, P.; Bertolucci, S.; Mooney, M.; Dytman, S.; Rosenberg, M.; Carranza, H.; et al. Calibration and simulation of ionization signal and electronics noise in the ICARUS liquid argon time projection chamber. *arXiv* **2024**, arXiv:2407.11925. [CrossRef]
10. Acciarri, R.; Adams, C.; Asaadi, J.; Baller, B.; Bolton, T.; Bromberg, C.; Cavanna, F.; Church, E.; Edmunds, D.; Ereditato, A.; et al. A study of electron recombination using highly ionizing particles in the ArgoNeuT Liquid Argon TPC. *J. Instrum.* **2013**, *8*, P08005. [CrossRef]
11. Abratenko, P.; Gurung, G.; Zennamo, J.; Richards, E.; Sapienza, P.; Bertolucci, S.; Mooney, M.; Dytman, S.; Rosenberg, M.; Carranza, H.; et al. Angular dependent measurement of electron-ion recombination in liquid argon for ionization calorimetry in the ICARUS liquid argon time projection chamber. *arXiv* **2024**, arXiv:2407.12969. [CrossRef]
12. Kashur, L.; Mueller, J. Muon Neutrino Reconstruction at ICARUS with Machine Learning. June 2024. Available online: https://agenda.infn.it/event/37867/contributions/228361/ (accessed on 9 December 2024).
13. Raselli, G.; Behera, B.; Benocci, R.; Bonesini, M.; Copello, S.; Diwan, M.; Menegolli, A.; Petrillo, G.; Prata, M.C.; Rossella, M.; et al. Time calibration and synchronization of the scintillation light detection system in ICARUS-T600. *J. Instrum.* **2024**, *19*, C01027. [CrossRef]
14. Abratenko, P.; Alterkait, O.; Andrade Aldana, D.; Anthony, J.; Arellano, L.; Asaadi, J.; Ashkenazi, A.; Balasubramanian, S.; Baller, B.; Barr, G.; et al. First demonstration of $\mathcal{O}(1\ \text{ns})$ timing resolution in the MicroBooNE liquid argon time projection chamber. *Phys. Rev. D* **2023**, *108*, 052010. [CrossRef]
15. Vicenzi, M. Reconstruction of the BNB and NuMI Neutrino Bunch Structure with ICARUS. July 2024. Available online: https://indico.fnal.gov/event/64626/contributions/294991/(accessed on 9 December 2024).
16. Drielsma, F.; Terao, K.; Dominé, L.; Koh, D.H. Scalable, end-to-end, deep-learning-based data reconstruction chain for particle imaging detectors. *arXiv* **2021**, arXiv:2102.01033.
17. Artero Pons, M. *Neutrino Reconstruction Analysis at ICARUS Detector*; Fermi National Accelerator Laboratory (FNAL): Batavia, IL, USA, 2024. [CrossRef]
18. Roy, P. *Status of ICARUS-NuMI Interaction Cross-Section Analysis*; Fermi National Accelerator Laboratory (FNAL): Batavia, IL, USA, 2024. [CrossRef]
19. Batell, B.; Berger, J.; Ismail, A. Probing the Higgs portal at the Fermilab short-baseline neutrino experiments. *Phys. Rev. D* **2019**, *100*, 115039. [CrossRef]
20. Co, R.T.; Kumar, S.; Liu, Z. Searches for heavy QCD axions via dimuon final states. *J. High Energy Phys.* **2023**, *2023*, 111. [CrossRef]
21. Alrahman, F.A.; Gurung, G.; Zennamo, J.; Richards, E.; Sapienza, P.; Bertolucci, S.; Mooney, M.; Wieler, F.A.; Dytman, S.; Rosenberg, M.; et al. Search for a Hidden Sector Scalar from Kaon Decay in the Di-Muon Final State at ICARUS. *arXiv* **2024**, arXiv:2411.02727.